

Substrate Binding Drives Large-Scale Conformational Changes in the Hsp90 Molecular Chaperone

Timothy O. Street,¹ Laura A. Lavery,¹ and David A. Agard^{1,2,*}

¹Department of Biochemistry and Biophysics

²Howard Hughes Medical Institute

University of California, San Francisco, San Francisco, CA 94158-2517, USA

*Correspondence: agard@msg.ucsf.edu

DOI 10.1016/j.molcel.2011.01.029

SUMMARY

Hsp90 is a ubiquitous molecular chaperone. Previous structural analysis demonstrated that Hsp90 can adopt a large number of structurally distinct conformations; however, the functional role of this flexibility is not understood. Here we investigate the structural consequences of substrate binding with a model system in which Hsp90 interacts with a partially folded protein ($\Delta 131\Delta$), a well-studied fragment of staphylococcal nuclease. SAXS measurements reveal that under apo conditions, Hsp90 partially closes around $\Delta 131\Delta$, and in the presence of AMPPNP, $\Delta 131\Delta$ binds with increased affinity to Hsp90's fully closed state. FRET measurements show that $\Delta 131\Delta$ accelerates the nucleotide-driven open/closed transition and stimulates ATP hydrolysis by Hsp90. NMR measurements reveal that Hsp90 binds to a specific, highly structured region of $\Delta 131\Delta$. These results suggest that Hsp90 preferentially binds a locally structured region in a globally unfolded protein, and this binding drives functional changes in the chaperone by lowering a rate-limiting conformational barrier.

INTRODUCTION

Hsp90 is a ubiquitous molecular chaperone. Originally identified in the heat shock response, Hsp90 plays important regulatory roles under nonstress conditions by its interactions with specific classes of substrates, such as kinases and nuclear receptors (Young et al., 2001). Consistent with being upregulated upon heat shock, Hsp90 can suppress thermal aggregation (Jakob et al., 1995; Wiech et al., 1992) and facilitate protein folding by reducing misfolding via interactions with aggregation-prone unfolding intermediates (Schneider et al., 1996). In vivo, Hsp90 receives unfolded proteins transferred from Hsp40/70 and receives specific classes of native or near-native substrates that are recruited by dedicated cochaperones. In eukaryotes, Hsp90's substrate interactions are highly regulated by cochaperones that modulate the Hsp90 ATPase activity; aid in substrate recruitment, maturation, or release; and target

substrates for degradation or intracellular trafficking. These important and multifaceted roles are reflected in Hsp90's high cellular abundance (2%–5% of cytosolic protein under nonstressed conditions). The in vivo characterized substrates (<http://www.picard.ch/>) have not been found to share a common sequence or structure motif and span an exceptionally wide range of sizes from α -synuclein to telomerase (14–290 kDa) (Falsone et al., 2009; Forsythe et al., 2001).

Recent structural work demonstrated that while Hsp90 is a dimer where each monomer has three well-folded and stable domains (N-terminal, middle, C-terminal), the overall molecule can adopt radically different conformations (Figure 1) in response to nucleotide and conditions. For example, under apo conditions, the Hsp90 from *E. coli*, HtpG, crystallized in a V-shaped conformation (Shiau et al., 2006) (ribbon structure, left panel, Figure 1), while in solution, a highly open conformation (blue surface structure) and a more closed conformation (red surface) are populated in a pH-dependent manner (Krukenberg et al., 2008, 2009b). The more closed state is similar to a crystal structure of the Hsp90 homolog specific to the endoplasmic reticulum, Grp94 (Dollins et al., 2007). The apo conformations largely differ by rigid-body rotation at the interface between the middle domain (MD) and C-terminal domain (CTD), creating a variable-sized cleft between the monomer arms; there is also N-terminal domain (NTD)-MD rotation, changing the NTD orientation. Addition of nonhydrolyzable ATP analogs such as AMPPNP results in closure to an NTD dimerized conformation (Ali et al., 2006) (Figure 1, central panel), while ADP transiently stabilizes a very compact state (Figure 1, right panel) (Shiau et al., 2006) (Southworth and Agard, 2008). Small-angle X-ray scattering (SAXS) and single-particle electron microscopy measurements have shown that multiple Hsp90 conformations coexist in a delicate equilibrium that can be shifted not only by nucleotide binding, but also by osmolyte and pH conditions (Krukenberg et al., 2009b; Southworth and Agard, 2008; Street et al., 2010). SAXS has been a powerful tool for characterizing the Hsp90 conformational ensemble (Bron et al., 2008; Krukenberg et al., 2008, 2009a, 2009b; Onuoha et al., 2008; Zhang et al., 2004) and has shown that the apo-state flexibility is universal in all homologs that have been examined (HtpG, Hsc82, hHsp90 α , Grp94, and TRAP) (Krukenberg et al., 2009a and unpublished data). However, the functional role of Hsp90 flexibility and conformational dynamics is not understood.

Indeed, despite the ubiquity of Hsp90 and the long list of in vivo identified substrates (known as client proteins), little is

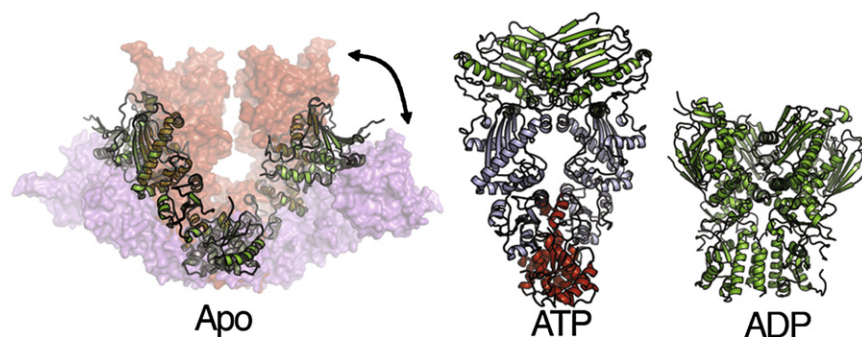


Figure 1. Conformational Flexibility of the Hsp90 Molecular Chaperone

The bacterial Hsp90 homolog, HtpG, crystallized in a V-shaped conformation (cartoon, left panel). SAXS measurements have demonstrated that, in solution, more extended and compact conformations are primarily populated, differing by rigid-body rotation at the junction between the middle and C-terminal domains. The closed “ATP” state (central panel) involves rigid rotation at the MC interface and additional rotation of the N-terminal domain (green), resulting in secondary dimer contacts. ADP transiently stabilizes a very compact state (right panel).

known about how Hsp90 makes these interactions. There is some evidence suggesting that substrate folding stability is linked to Hsp90 binding. Hsp90 has a much stronger *in vivo* interaction with the highly destabilized v-Src versus c-Src (otherwise having 98% sequence identity) (Taipale et al., 2010), NMR studies of p53 indicate that human Hsp90 only binds after substrate unfolding (Rudiger et al., 2002), and HtpG has been found to bind an unfolded ribosomal protein, L2 (Motojima-Miyazaki et al., 2010). Indeed, the ability of Hsp90 to interact with and shift the equilibrium between metastable conformations is thought to play a role in Hsp90 in transitioning the glucocorticoid receptor between apo and ligand-bound states, which requires a large conformational change. These observations suggest that Hsp90/substrate interactions may be enhanced by reducing substrate stability to favor partially structured or metastable conformations. This approach is technically challenging because for most proteins, partially folded states are difficult to populate and are prone to misfolding and aggregation.

One protein system that is amenable to this approach is the well-characterized staphylococcal nuclease (SN). Extensive studies have shown that a 131-residue fragment of SN ($\Delta 131\Delta$; full length is 149 residues) is globally unfolded but remains compact, with residual structured regions (Shortle, 2002; Alexandrescu et al., 1994; Alexandrescu and Shortle, 1994; Wang and Shortle, 1995). Indeed, $\Delta 131\Delta$ and other similarly destabilized SN variants are close in free energy to the native state, as indicated by the fact they can be effectively refolded with tight binding inhibitors and stabilizing osmolytes (Baskakov and Bolen, 1998; Wang et al., 1995). $\Delta 131\Delta$ is monomeric at high concentrations, stable under a wide variety of conditions, and amenable to NMR, all of which has made it an ideal model system to investigate structural properties of unfolded proteins (Shortle, 2002). Here, we test $\Delta 131\Delta$ as a model system to investigate Hsp90/substrate interactions. Using a combination of SAXS, FRET, binding anisotropy, and NMR, we find that Hsp90 binds a structured region of $\Delta 131\Delta$, which results in conformational and functional changes in the chaperone.

RESULTS

To determine Hsp90's binding affinity for $\Delta 131\Delta$, we labeled a cysteine variant of $\Delta 131\Delta$ with the IAEDANS fluorophore to measure fluorescence polarization anisotropy. The Perrin equation estimates of the rotational correlation times for $\Delta 131\Delta$ and

HtpG (5 and 55 ns) span the IAEDANS excited state lifetime (10–15 ns), suggesting that binding will significantly increase polarization anisotropy. Indeed, upon addition of the bacterial Hsp90, HtpG, the fluorescence anisotropy of IAEDANS-labeled $\Delta 131\Delta$ increases substantially (Figure 2A). The concentration series is well-fit by single-site noncooperative binding (solid lines), resulting in a dissociation constant (K_D) of 9 μM . Similar binding curves were measured for the yeast Hsp90 homolog (K_D of 6 μM), whereas addition of BSA resulted in minimal anisotropy changes (data not shown). Anisotropy titration measurements show saturation near a 1:1 stoichiometry (Hsp90 dimer: $\Delta 131\Delta$) (Figure S1A).

Previous studies have shown that unfolded SN fragments can be refolded in the presence of CaCl_2 and a tight binding inhibitor, thymidine 3',5'-bisphosphate (pdTp) (Shortle and Meeker, 1989). We used these stabilizers to refold IAEDANS-labeled $\Delta 131\Delta$ and found that HtpG no longer significantly increases fluorescence anisotropy, demonstrating that HtpG is binding a globally unfolded state. However, as discussed later, HtpG selectively interacts with a highly structured region within the unfolded protein.

The micromolar concentration range for binding precludes structural analysis by electron microscopy, which for Hsp90 is performed at ~ 100 nM, whereas SAXS measurements are ideally suited for this concentration regime. Previous studies have shown that SAXS measurements can be used to determine the multistate conformational equilibrium of Hsp90. For these experiments, X-ray scattering intensity was measured between Q values ($4\pi\sin\theta/\lambda$, where 2θ is the scattering angle) of 0.01–0.3 \AA^{-1} , radially averaged and buffer subtracted. The resulting data were transformed to an interatomic distance distribution, $P(r)$, using the GNOM program (Svergun, 1991). The $P(r)$ distribution of HtpG alone has significant magnitude at large distances (Figure 2B), indicative of a substantial open-state population, very similar to other measurements of HtpG at pH 7.5 (Krukenberg et al., 2009b). Subsequent addition of $\Delta 131\Delta$ shows a conformational change; a concentration series with increasing $\Delta 131\Delta$ results in a systematic contraction in the $P(r)$ distribution (Figure 2B). These changes reflect a transition to more compact Hsp90 conformations that saturate near a 1:1 stoichiometry (Hsp90 dimer: $\Delta 131\Delta$). The Guinier analysis of low-Q scattering is linear for all concentrations measured (data not shown), indicating no significant aggregation.

Similar $\Delta 131\Delta$ -induced contractions are observed in the $P(r)$ distributions for the yeast and human Hsp90 homologs (Figures

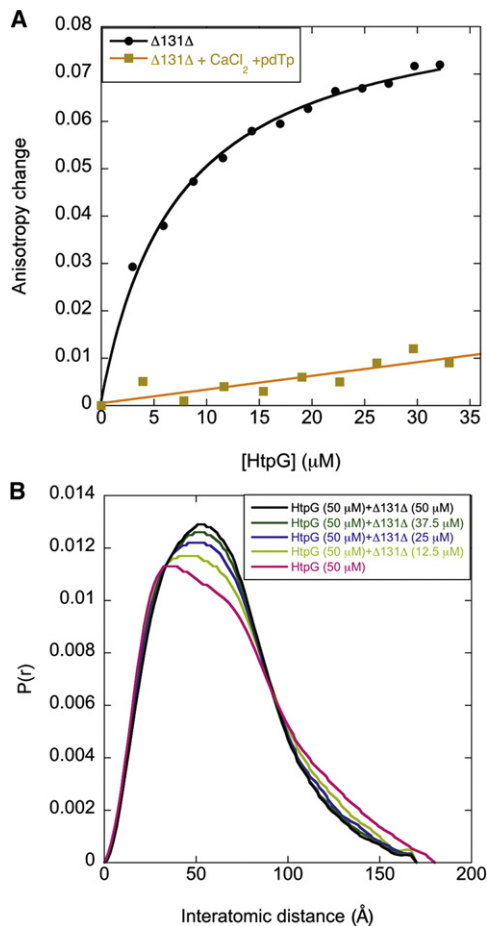


Figure 2. HtpG Binds $\Delta 131\Delta$, Resulting in a Conformational Change

(A) IAEDANS-labeled $\Delta 131\Delta$ undergoes a significant increase in anisotropy upon addition of HtpG. In contrast, in the presence of 10 mM CaCl_2 and 5 mM pdTp binding is negligible. The curve is fit with noncooperative hyperbolic binding (solid lines).

(B) Scattering curves are shown for HtpG with increasing concentration of $\Delta 131\Delta$. The $P(r)$ curve, which summarizes the relative probability of interatomic scattering distances, contracts with increasing $\Delta 131\Delta$. Conditions: 25 mM TRIS (pH 7.5), 25 mM KCl, 10 mM MgCl_2 .

S1B and S1C). Their contractions are smaller than for HtpG, which is consistent with previous SAXS and electron microscopy measurements that show the yeast and human homologs more strongly favor the open state relative to HtpG in the absence of nucleotide (Southworth and Agard, 2008). The substrate-induced conformational change is specific to unfolded SN, addition of folded wild-type SN results in no significant conformational change, and the scattering of SN and HtpG are independent and additive (Figures S2A and S2B).

Apo Hsp90 Partially Closes around $\Delta 131\Delta$

The measured SAXS change in response to $\Delta 131\Delta$ (Figure 2B) has two contributions: (1) additional scattering from bound $\Delta 131\Delta$ and (2) altered scattering from chaperone contraction. As discussed below, we separated out these contributions by

first determining the location of $\Delta 131\Delta$ on HtpG subdomains using ab initio reconstructions and then applying structure-based fitting and rigid-body analysis to determine the chaperone conformation.

To locate $\Delta 131\Delta$ on HtpG, we first examined a subdomain containing the N-terminal and middle domains (NM, residues 1–495). This monomeric fragment behaves as a rigid object and is significantly smaller than the HtpG dimer, increasing the relative signal from $\Delta 131\Delta$ scattering in the complex. We used the DAMMIN and MONSA programs (Svergun, 1999) to generate ab initio molecular envelopes from the NM/ $\Delta 131\Delta$ scattering curve (Figure S2C) for use as a starting point for modeling scattering from the full-length HtpG dimer. DAMMIN determines an envelope from exhaustive rearrangement and Monte-Carlo minimization of dummy atoms to match the experimentally determined distance distribution. MONSA simultaneously fits scattering data of complexes and individual subcomponents to determine the location of members within a complex. No initial model was used, and yet the resulting DAMMIN volume for the NM domain alone matches well with the expected structure (upper left panel, Figure 3A).

The MONSA reconstruction shows that $\Delta 131\Delta$ (cyan volume, Figure 3A, upper right) binds predominantly at the middle domain. Multiple repeated MONSA runs were very similar (Figure S2D). The DAMMIN and MONSA envelopes for the NM/ $\Delta 131\Delta$ complex are broadly consistent with small local differences (Figure S2E); the additional information from simultaneous fitting used in MONSA provides higher-resolution information versus DAMMIN. The conclusion that $\Delta 131\Delta$ binds at a terminal region of the NM domain is evident from the primary scattering data, which show that the addition of $\Delta 131\Delta$ results in a relative increase in long-range scattering distances (Figure S2C). When the MONSA reconstruction is mapped back on the full-length HtpG structure, $\Delta 131\Delta$ is found to project between the monomer arms (Figure 3A). Although these reconstructions provide a starting point for analyzing the SAXS data from the full-length HtpG/ $\Delta 131\Delta$ complex, it should be noted that the reconstructions are of too low resolution to conclude whether $\Delta 131\Delta$ binding is restricted to the MD or whether additional contacts are made to the NTD.

To analyze the SAXS data from the full-length HtpG/ $\Delta 131\Delta$, we first examined whether any of the four dominant HtpG conformations (open, ATP, Grp94, and V-shaped) could satisfactorily describe the chaperone conformation upon binding $\Delta 131\Delta$. For reference, previous studies showed that HtpG's conformational ensemble could be determined by linear combination fitting of SAXS data with different structural states (Krukenberg et al., 2009a). In the absence of $\Delta 131\Delta$ and at pH 7.5, HtpG adopts an 81%/19% open/Grp94 equilibrium, resulting in a good fit to the chaperone-alone data (blue squares, Figure 3B) and is quantified by a low R factor of 2.2% (see equation in Experimental Procedures). Single HtpG conformations fit the HtpG/ $\Delta 131\Delta$ scattering poorly (Figure S3A), with R factors of 23%, 24%, 17%, and 17% for the open, ATP, Grp94, and V-shaped conformations, respectively. Inspection of Figure S3A shows that any combination of ATP, Grp94, and V-shaped conformations would fit the experimental data poorly due to the lack of long-range scattering distances above 120 Å. By

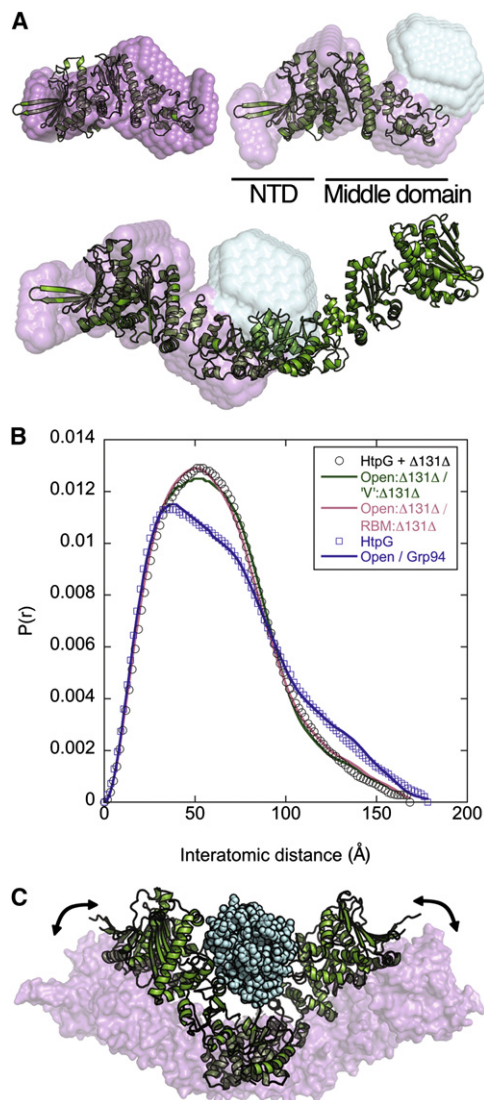


Figure 3. Contraction of HtpG upon Binding $\Delta 131\Delta$

(A) The NM domain DAMMIN reconstruction (upper left panel, magenta surface) matches well with the expected structure (cartoon). The MONSA reconstruction of the NM/ $\Delta 131\Delta$ complex shows that $\Delta 131\Delta$ (right panel, cyan surface) binds on the middle domain toward the C terminus. This reconstruction allows the $\Delta 131\Delta$ volume to be mapped back on full-length HtpG, revealing that $\Delta 131\Delta$ projects toward the dimer cleft.

(B) Scattering for HtpG alone (blue squares) is well fit with a simple two-state model involving the open/Grp94 states (blue line). Scattering from HtpG/ $\Delta 131\Delta$ (black circles) was fit by the open/V-shaped states and the open/rigid-body model (RBM), which both fit the data well.

(C) This analysis shows that HtpG contracts to a V-shaped conformation with $\Delta 131\Delta$ (cyan spheres) projecting between the monomer arms. This conformation remains in equilibrium with the open state (magenta surface).

contrast, a 58%/42% linear combination of open/V-shape provides a better description of the SAXS data (Figure S3A), indicating that HtpG remains in a conformational equilibrium upon $\Delta 131\Delta$ binding, but now with the V-shaped conformer.

To account for scattering from bound $\Delta 131\Delta$, we generated structural models of HtpG: $\Delta 131\Delta$ complexes with 131 residues

of SN attached to the HtpG middle domain, based on the MONSA reconstruction (see Experimental Procedures). For the open and crystallographic V-shaped conformations, this addition significantly decreased R factors (from 23% to 13% for the open state and from 17% to 11% for the V-shaped conformation), whereas for the Grp94 and ATP conformations, this addition resulted in higher R factors. Indeed, a 51%/49% linear combination of the open: $\Delta 131\Delta$ /V: $\Delta 131\Delta$ states fit the scattering data well (Figure 3B) (R factor of 3.8%). The relative contributions from the open and V-shaped states to the $P(r)$ fit are shown in Figure S3B. All SAXS fitting statistics are summarized in Table S1. Although the MONSA analysis suggests that $\Delta 131\Delta$ binds predominantly at the MD, as an additional check we generated structural models with $\Delta 131\Delta$ located at different NTD positions and confirmed with linear combination fitting with the open state that this positioning resulted in a poorer fit to the data (Figure S3C).

The above results indicate that HtpG adapts its conformation by partially closing around $\Delta 131\Delta$. To best determine the chaperone conformation in this state, we performed rigid-body analysis. Since the open/V-shaped/Grp94 conformations of HtpG differ primarily by the opening angle between the middle and C-terminal (MC) domains (Figure 1), the Grp94 conformation can be used as a starting point in a rigid-body minimization, where the MC angle is systematically explored for an optimal fit to the scattering data. To ensure robustness, we performed this analysis by simultaneously fitting four data sets with varying ratios of open and $\Delta 131\Delta$ -induced closure (see Experimental Procedures). This analysis confirms that a V-shaped structure is favored, very similar in opening angle to the crystallographically determined structure (comparison shown in Figure S4C). The rigid-body model (RBM) in equilibrium with the open state (Figure 3C) results in a good fit, with an R factor of 3.4% (Figure 3B). The remaining three data sets used in the simultaneous fitting have similarly low R factors (Table S1) (1.9%, 1.9%, and 3.3%). Since the RBM does not allow for the NTD rotation observed in the ATP conformation, we also confirmed that an ATP: $\Delta 131\Delta$ /open: $\Delta 131\Delta$ combination does not fit the data (R factor of 7.3%).

Influence of $\Delta 131\Delta$ on the Hsp90 Nucleotide Cycle

In the presence of AMPPNP, Hsp90 undergoes a dramatic closure involving N-terminal dimerization (Figure 1). For HtpG at pH 7.5, previous studies showed that saturating AMPPNP drives only a partial population shift to the ATP conformation (Krukenberg et al., 2009a). Since the ATP conformation is marginally populated, it is sensitive to whether $\Delta 131\Delta$ binds favorably; if $\Delta 131\Delta$ favors/disfavors binding the closed state, then an increase/decrease in closure is expected. Indeed, in the presence of 10 mM AMPPNP, we find that $\Delta 131\Delta$ increases closure, which results in a $P(r)$ distribution very different from that observed under apo conditions (Figure 4A). To quantify the relative populations of different states, we again used linear combination fitting, utilizing the structural models based on the previous MONSA analysis (Figure 4B). This fitting shows an approximately 2-fold increase in the ATP state population (from 39% to 70%) (Table S1).

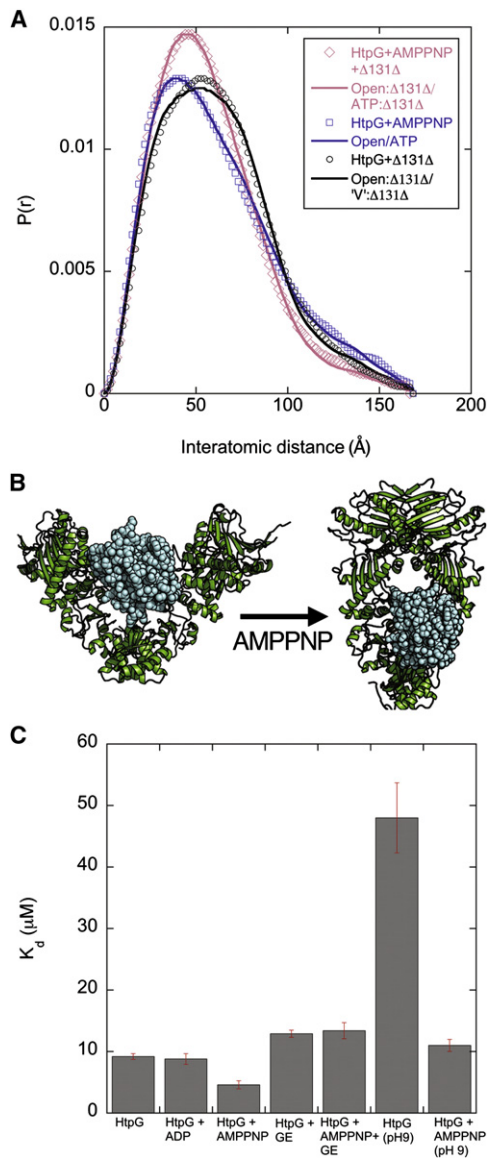


Figure 4. Nucleotide Dependence of Δ 131 Δ Binding

(A) In the presence of 10 mM AMPPNP, HtpG's $P(r)$ distribution is shifted toward smaller distances, reflecting an increase in the population of the ATP conformation (blue squares). The subsequent addition of Δ 131 Δ (gray diamonds) increases the ATP conformation from 39% to 70% (fits shown in solid lines). The influence of Δ 131 Δ on HtpG under AMPPNP conditions differs significantly from apo conditions (black circles).

(B) The open/ATP structural transition differs by a significant change in chaperone conformation.

(C) Fluorescence anisotropy measurements show an increase in binding affinity under AMPPNP conditions. Bars represent the standard error of the mean. Geldanamycin (GE) and nucleotide concentrations were 250 μ M and 5 mM; other buffer conditions are same as Figure 2.

Consistent with the above observations, we find that the binding affinity between HtpG and Δ 131 Δ is enhanced 2-fold by AMPPNP (Figure 4C). This enhancement is blocked by a competitive inhibitor, geldanamycin (GE); the small increase

in K_D from GE is from the DMSO storage buffer, which alone increases the K_D . These results predict that the effect of AMPPNP on the binding affinity for Δ 131 Δ should be most pronounced at pH 9, where HtpG undergoes a full population shift from the most open state to the ATP conformation (Krukenberg et al., 2009a). Indeed, at pH 9 there is a 5-fold increase in binding affinity for Δ 131 Δ upon addition of AMPPNP. Under both apo and AMPPNP conditions, binding is pH dependent over the neutral range (pH 6–9), suggesting the involvement of a histidine. There is a strong salt dependence to Δ 131 Δ binding K_D and the resulting conformational equilibrium in HtpG: Δ 131 Δ (Figures S4A and S4B), suggesting an electrostatic contribution. This conformational variation was useful in performing the rigid-body minimization of multiple data sets, as discussed earlier (see Experimental Procedures).

In contrast to AMPPNP, there is a negligible influence of ADP on binding. Previous electron microscopy measurements have identified a compact HtpG conformation in the presence of ADP (Shiau et al., 2006; Southworth and Agard, 2008), yet this state is only transiently populated under SAXS experimental conditions (Krukenberg et al., 2008). Our results therefore suggest that under our experimental conditions, the ADP state is insufficiently populated to affect the bulk binding of Δ 131 Δ .

Since Δ 131 Δ affects the apo/ATP equilibrium, it either accelerates closure or slows reopening. We tested this prediction with FRET, since the Buchner and Hugel labs have showed that the open/ATP kinetics can be monitored this way (Hessling et al., 2009; Mickler et al., 2009). Following their work, we generated heterodimers of HtpG labeled with Alexa Fluor 647 and Alexa Fluor 555 at positions 62 and 341 on opposite monomers (see Experimental Procedures). FRET measurements were performed at pH 9 because under these conditions, HtpG undergoes a complete open/ATP population shift (Krukenberg et al., 2009a). Indeed, under apo conditions there is minimal FRET, whereas after an extended incubation with AMPPNP, there is significant FRET, as indicated by an increase/decrease in acceptor/donor fluorescence (Figure 5A).

The large change in acceptor fluorescence at 664 nm provides a sensitive assay for closure kinetics. As shown in Figure 5B (red circles), upon addition of AMPPNP there is a slow increase in acceptor fluorescence, with single exponential kinetics similar to those measured with the yeast Hsp90 homolog (Hessling et al., 2009). When Δ 131 Δ is incubated with HtpG prior to addition of AMPPNP, nucleotide-driven closure is accelerated 5-fold (Figure 5B, green squares), similar to the affinity enhancement measured by anisotropy at pH 9. As a control, we tested the influence of BSA and the folded wild-type SN (both at 50 μ M, the same concentration that was used with Δ 131 Δ) on closure kinetics and found no significant change (not shown). In contrast to closure kinetics, Δ 131 Δ has no effect on reopening from the closed state (Figure S5A). The closure acceleration by Δ 131 Δ implies that hydrolysis should also be accelerated, which we tested with a previously described assay (see Experimental Procedures). At 50 μ M Δ 131 Δ , the hydrolysis rate is increased 4-fold (Figure S5B). The increase in hydrolysis is specific to Δ 131 Δ 's influence on HtpG, as this increase can be abolished by 200 μ M radicicol.

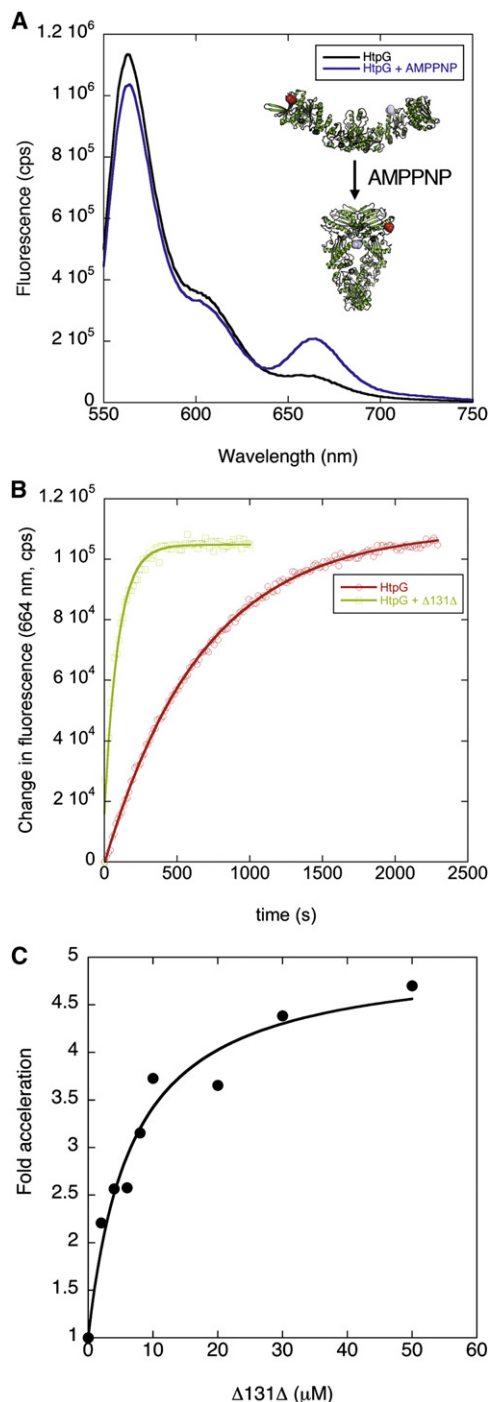


Figure 5. Substrate Binding Accelerates Nucleotide-Driven Closure

(A) FRET measurements of apo (black) and AMPPNP (blue) HtpG show an increase/decrease in acceptor/donor fluorescence at 664 and 563 nm, respectively. These changes reflect the dramatic change in fluorophore distance between the open and ATP states (cartoon, red and blue spheres show the fluorophore locations at residues 62 and 341).

(B) Closure is 5-fold accelerated by $\Delta 131\Delta$. Single exponential fits are shown in solid lines.

(C) The $\Delta 131\Delta$ concentration dependence on closure acceleration shows a noncooperative relationship between $\Delta 131\Delta$ binding and closure.

The SAXS modeling and anisotropy data suggest a single bound $\Delta 131\Delta$ per HtpG dimer. This predicts a noncooperative concentration dependence of the $\Delta 131\Delta$ -induced closure acceleration, in contrast to a two-site cooperative model in which an initial quadratic dependence on $\Delta 131\Delta$ concentration would be expected. Indeed, the $\Delta 131\Delta$ -induced closure acceleration (Figure 5C) has a simple rectangular hyperbolic concentration dependence (solid line).

HtpG Binds a Locally Structured Region on $\Delta 131\Delta$

A significant advantage of using $\Delta 131\Delta$ as a model system is that it is amenable to NMR measurements. To gain a higher-resolution picture of the interaction site on $\Delta 131\Delta$, we measured the $\Delta 131\Delta$ HSQC with and without HtpG. The original assignment of $\Delta 131\Delta$ was performed at low pH, high temperature, and the absence of buffer, salt, and magnesium chloride (Alexandrescu and Shortle, 1994), under which conditions HtpG is not stable. However, the majority of the peaks remain, and at similar chemical shifts at pH 6.0, 25 mM MES, 25 mM KCl, and 5 mM $MgCl_2$ (Figure 6A, left panel). The transferred $\Delta 131\Delta$ assignments under these conditions were confirmed with HNCA and CBCA(CO)NH measurements on double-labeled sample. Of the 131 residues of $\Delta 131\Delta$, 41 residues could be unambiguously assigned, allowing us to monitor their response to HtpG.

Nonspecific contacts between HtpG and $\Delta 131\Delta$ would result in a uniform loss of NMR signal across the $\Delta 131\Delta$ sequence; however, at stoichiometric concentrations of HtpG and $\Delta 131\Delta$, we observe that a subset of peaks disappear, while others have reduced intensity (Figure 6A, right panel). The fractional loss of peak height across different positions of the $\Delta 131\Delta$ sequence is HtpG concentration dependent and shows a clear trend, where locations near $\Delta 131\Delta$ residue 100 are highly impacted by the addition of HtpG, whereas more distant positions are less affected (Figure 6B). The region from residues 85–110 is completely broadened at stoichiometric concentrations of Hsp90. There is a roughly monotonic increase in peak height at increasing sequence distance away from the region that loses complete peak intensity, which suggests that chain mobility restricted by HtpG binding is relieved with increasing chain length from the binding site due to lack of structure in $\Delta 131\Delta$. No new peaks were observed upon addition of HtpG, as expected for their complete broadening, due to the slow tumbling of the interface region of $\Delta 131\Delta$ in complex with HtpG.

Significantly, the region with maximal peak loss (residues 85–110) has been identified as the most structured region within the globally unfolded protein. In particular, the helix between residues 97–107 has been shown to have significant structure, as well as two turns located at residues 83–86 and 94–97 (Alexandrescu et al., 1994; Alexandrescu and Shortle, 1994; Wang and Shortle, 1995). Relaxation measurements have shown that this region has high-order parameters and positive NOEs, again indicative of significant structure (Alexandrescu and Shortle, 1994; Ohnishi and Shortle, 2003).

DISCUSSION

Hsp90:client interactions have proven difficult to study in vitro, likely because the chaperone favors interactions with partially

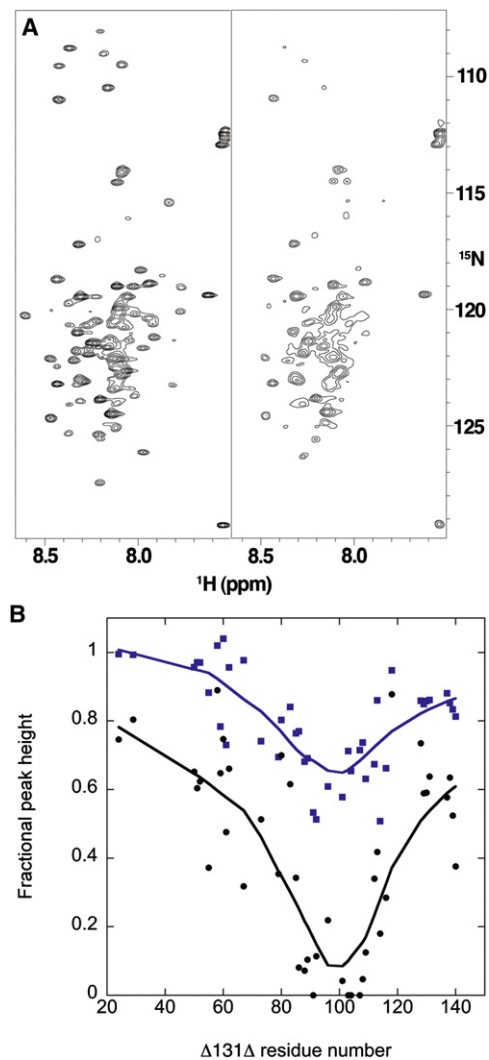


Figure 6. HspG Binds a Specific Region on $\Delta 131\Delta$

(A) The HSQC of $\Delta 131\Delta$ has 41 peaks that can be unambiguously assigned. Addition of an equimolar concentration of HspG results in peak height reduction for many but not all of the $\Delta 131\Delta$ residues.

(B) Peaks for different $\Delta 131\Delta$ residues are differentially affected by HspG. At 1:10 and 1:1 concentration ratios (HspG: $\Delta 131\Delta$, blue squares and black circles), residues 85–110 are most affected, whereas residues are progressively less affected away from this region. Solid lines are interpolations.

folded or metastable client states that are only transiently populated. Here, our aim has been to test the use of a model system of nonnative states for probing Hsp90:substrate interactions. Our choice of system was guided by the fact that, although globally unfolded, $\Delta 131\Delta$ has significant residual structure, is only marginally unstable, but is soluble and nonaggregating even at high concentrations. Using a combination of SAXS, FRET, fluorescence anisotropy, and NMR, we have found that HspG binds a specific region of $\Delta 131\Delta$, and this binding results in large-scale conformational and functional changes to the chaperone. These findings reveal basic steps in the Hsp90: $\Delta 131\Delta$ nucleotide cycle (Figure 7).

Our SAXS measurements and modeling suggest that under apo conditions, HtpG adapts its conformation to $\Delta 131\Delta$ by a partial closure (Figure 3C). This structural analysis was aided by localizing $\Delta 131\Delta$ with ab initio reconstructions prior to structure-based fitting and rigid-body analysis. The SAXS fitting on full-length HtpG shows that, upon binding $\Delta 131\Delta$, the chaperone adopts an equilibrium between a V-shaped conformation and a fully open state (Figure 3C and Table S1), indicating that Hsp90 maintains significant flexibility even after substrate loading. The residual flexibility suggests that Hsp90 could accommodate other cochaperones or binding partners within the loaded conformation. Also, to advance through the nucleotide cycle, Hsp90 must undergo large conformational changes requiring significant structural plasticity to reach the ATP state. While our SAXS modeling suggests that $\Delta 131\Delta$ remains bound to roughly the same region on HtpG, it is likely that, concomitant with HtpG closure, there is some alteration in $\Delta 131\Delta$:HtpG interactions and perhaps in $\Delta 131\Delta$ structure.

The apo, substrate-bound conformation of Hsp90 has a significant impact on the kinetics of the nucleotide cycle. Following previous work (Hessling et al., 2009; Mickler et al., 2009), we used kinetic FRET measurements to show that closure to the ATP state is significantly accelerated by $\Delta 131\Delta$ (Figure 5). This closure acceleration is paralleled by an ATPase acceleration (Figure S5B), similar to reports of ATPase stimulation of human Hsp90 by the ligand binding domain of the glucocorticoid receptor (McLaughlin et al., 2002). Our findings suggest that closure is rate limiting in ATP hydrolysis by Hsp90 and that client binding activates the chaperone by lowering this rate-limiting conformational barrier. The coupling between client binding, Hsp90 conformational changes, and subsequent ATP hydrolysis suggests a simple mechanism by which Hsp90 restricts unnecessary ATP utilization while maximizing efficiency of client activation.

The ATP state transition involves numerous structural changes: ATP binding restructures an N-terminal helical region that (1) makes cross-monomer contacts; (2) dramatically changes the NTD/MD orientation, leading to an interaction between a highly conserved arginine (residue 336 in HtpG) and the ATP γ -phosphate; and (3) is associated with the release of a β strand that is swapped across monomers, stabilizing N-terminal dimerization; however, it is not known which of these processes (or others) are rate limiting. Indeed, our SAXS measurements are of too low resolution to conclude whether $\Delta 131\Delta$ contacts are restricted to a single monomer or whether $\Delta 131\Delta$ -induced closure is driven by cross-monomer contacts. A detailed study is needed to address these points.

The results with $\Delta 131\Delta$ suggest that Hsp90's conformational plasticity is functionally important and may allow it to adapt to structurally diverse substrates, which catalyze further structural changes that lead to ATP hydrolysis. This implies that Hsp90's flexibility should be conserved, which is indeed true for the homologs investigated by SAXS (HtpG, Hsc82, hHsp90a, Grp94, and TRAP) (Krukenberg et al., 2009a and unpublished data). For bacterial, yeast, and human Hsp90, detailed electron microscopy measurements have shown that a three-state apo-ATP-ADP conformational cycle is conserved, but that the equilibrium between states is species specific (Southworth and

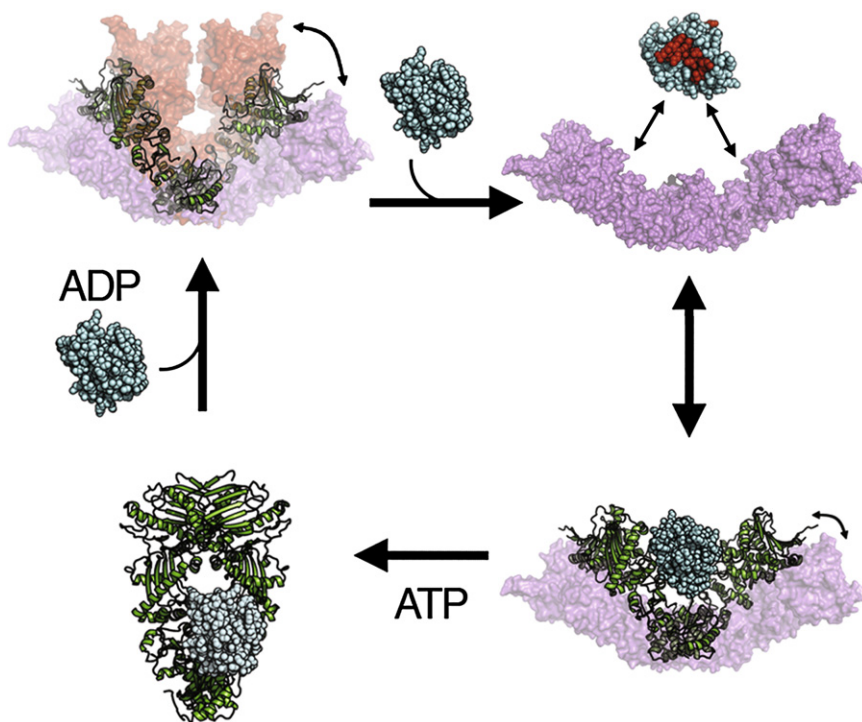


Figure 7. Hsp90 Chaperone Cycle for $\Delta 131\Delta$

Under apo conditions, Hsp90's flexibility allows for efficient substrate loading by structural accommodation. This substrate-loaded state accelerates closure to the ATP conformation and subsequent hydrolysis.

although SAXS measurements are ideal for characterizing the flexible Hsp90 conformation and the influence of $\Delta 131\Delta$, high-resolution measurements are needed to elucidate these molecular details.

EXPERIMENTAL PROCEDURES

The expression and purification of Hsp90 homologs and variants as well as $\Delta 131\Delta$ has been described previously (Alexandrescu et al., 1994; Cunningham et al., 2008; Krukenberg et al., 2008; Southworth and Agard, 2008). SAXS measurements were performed at the SIBYLS beamline (12.3.1) at the Advanced Light Source in Berkeley. Scattering was measured with 0.5, 2, and 5 s integrations and buffer subtracted. The radial intensity was converted to the $P(r)$ representation with the GNOM program

(Svergun, 1991). D_{max} cut-off values were selected manually to achieve smooth tails at high distance values.

SAXS Analysis

DAMMIN (Svergun, 1999) reconstructions used spherical starting models with no symmetry constraints. MONSA (Svergun, 1999) reconstructions used simultaneous fitting on multiple data sets (the NM domain and the NM/ $\Delta 131\Delta$ complex), keeping the $\Delta 131\Delta R_g$ fixed at 18 Å. The SUBCOMP program was used to align structures into DAMMIN and MONSA reconstructions. To approximate scattering from $\Delta 131\Delta$, 131 residues of an SN crystal structure (1STN) were appended to the middle domains of the crystallographically solved V-shaped conformation (2IOQ) as well as the open, Grp94, and ATP conformations. This was achieved by aligning HtpG conformations to the NM/ $\Delta 131\Delta$ MONSA envelope and positioning SN to avoid steric clash with HtpG. All HtpG conformations are available for download (<http://www.msg.ucsf.edu/agard/>).

Structure-based fitting and rigid-body analysis of SAXS data was performed with the PRFIT program, described previously (Krukenberg et al., 2009b). The quality of fit is quantified by an R factor:

$$R = \sum ||P_{obs}(r) - |P_{calc}(r)|/|P_{obs}(r)||$$

For rigid-body analysis, the NM domain of HtpG was allowed to pivot against residue 500 using computational methods described previously (Krukenberg et al., 2008, 2009a, 2009b). General three-axis rotational motion around this pivot started with a course step size of 10° and then was refined with 1° steps. The attached 131 residues of SN were included on a single monomer arm. The rigid-body fitting was simultaneously performed on multiple data sets with varying levels of $\Delta 131\Delta$ -induced closure. Specifically, we used a salt series that titrates the binding affinity and degree of closure (Figures S4A and S4B) and a previously characterized HtpG variant (H446K) that favors the Grp94 conformation (Krukenberg et al., 2009a). If the V-shaped conformation is a robust solution, then the rigid-body search will independently identify this state in these diverse data sets. To determine the

Agard, 2008). This result suggested that the Hsp90 conformational equilibrium is tuned to the specific substrate/cochaperone requirements of each organism. Indeed, $\Delta 131\Delta$ binds to the bacterial, yeast, and human Hsp90 homologs and affects their conformations; however, the relative magnitudes of these structural changes are species specific (Figure S1).

The conformational diversity and large structure of Hsp90 suggests that it can provide a combinatorial set of binding surfaces and conformations for interacting with structurally diverse substrates. An electron microscopy reconstruction of an Hsp90-Cdc37-Cdk4 complex (Vaughan et al., 2006) shows that Hsp90 adopts a more closed conformation than we observe with $\Delta 131\Delta$. This observation suggests that different substrates and cochaperone complexes can be accommodated by different Hsp90 conformations and possibly have different nucleotide cycle dependences.

Our NMR measurements suggest that Hsp90 selectively interacts with a region of $\Delta 131\Delta$ (residues ~85–110) that has been shown to have significant structure despite the fact that $\Delta 131\Delta$ is globally unfolded (Alexandrescu et al., 1994; Alexandrescu and Shortle, 1994; Ohnishi and Shortle, 2003; Wang and Shortle, 1995). Hsp90 is often referred to as operating in later stages of client folding, consistent with this finding. Future studies will be required to reveal whether binding changes the structure within this region, which specific elements of Hsp90 are involved in binding, and the impact of nucleotide-induced conformational changes in Hsp90. Inspection of the fractional peak height distribution in Figure 6B also shows decreased peak heights toward the C terminus of $\Delta 131\Delta$, possibly indicating a second binding site. Clearly,

robustness of the SAXS modeling, limiting cases with zero or two bound $\Delta 131\Delta$ were investigated and indeed only modestly affect fitted parameters (range shown in brackets in Table S1), as expected, given the small size of $\Delta 131\Delta$ relative to HtpG.

Fluorescence Measurements

Fluorescence anisotropy was measured on a Jobin Yvon fluorometer with excitation and emission monochromator slits both set to 5 nm, an integration time of 2 s, and excitation/emission wavelengths of 340/480 nm. A 5-fold molar excess of IAEDANS (Invitrogen) was used to label a cysteine variant of $\Delta 131\Delta$, K16C, at room temperature for 1 hr, and free dye was removed by extensive dialysis. Measurements with nucleotides and GE were pre-equilibrated for at least 20 min. Binding stoichiometry measurements were performed at 50 μM $\Delta 131\Delta$, with only a small concentration, 500 nM, labeled with IAEDANS.

FRET measurements were performed on the same fluorometer. A 5-fold molar excess of dye (Alexa Fluor 647 and Alexa Fluor 555, Invitrogen) was incubated with HtpG variants E62C and D341C for 3 hr at room temperature. HtpG has no native cysteines. The reaction was quenched with 2-fold excess of BME over dye. Free dye was separated by extensive dialysis and G50 size-exclusion chromatography (Roche). HtpG heterodimers (250 nM at a 1:1 stoichiometry) were formed by incubation for 30 min at 30°C. FRET measurements had 250 nM of heterodimer at a 1:1 stoichiometry. Closure was initiated by manual mixing of 5 mM AMPPNP, and reopening was initiated by subsequent addition of 50 mM ADP. The excitation and emission slits were 2 and 3 nm, with an integration time of 0.3 s. To control for photobleaching and burst-phase fluorescence, separate reactions without nucleotide were monitored and subtracted from nucleotide-containing samples.

ATPase Measurements

ATP hydrolysis was measured by a phosphate release assay described previously (Cunningham et al., 2008). Briefly, 1 μM of HtpG dimer was incubated with 50 μM $\Delta 131\Delta$ at pH 9, 50 mM KCl, and 5 mM MgCl_2 at 22°C and assayed for radiolabeled ^{32}P release. ATP (5 mM) was used with 0.8 pM of radiolabeled ATP. Negligible background ATPase was confirmed by addition of 200 μM radicol. Free P_i was separated from ATP and ADP by thin-layer chromatography. Spot imaging was performed on a Typhoon Imager (GE Healthcare) and was quantified with the ImageQuant program (GE Healthcare).

NMR Analysis

Isotopically labeled $\Delta 131\Delta$ was produced by a 10 ml overnight starter culture, which was spun down and washed in M9 minimal growth medium and then resuspended in 1 l of M9 media supplemented with 1 g/l ^{15}N ammonium chloride and 0.5 g/l isogrow growth supplement (Sigma). Uniformly labeled ^{13}C , ^{15}N samples were derived similarly with 1 g of ^{13}C glucose per liter of media. HSQC measurements were performed on a Bruker Avance 800 with $\Delta 131\Delta$ concentration of 200 μM . HNCA and CBCA(CO)NH measurements were performed on an Avance 500. Data were processed with NMRPipe (Delaglio et al., 1995), and peak height analysis was performed with the ccpn analysis software (<http://www.ccpn.ac.uk>). The $\Delta 131\Delta$ assignment was transferred from a previously published study of $\Delta 131\Delta$ (Alexandrescu and Shortle, 1994) and confirmed with the HNCA and CBCA(CO)NH experiments.

SUPPLEMENTAL INFORMATION

Supplemental Information includes five figures and one table and can be found with this article online at doi:10.1016/j.molcel.2011.01.029.

ACKNOWLEDGMENTS

We thank David Shortle for kindly providing the $\Delta 131\Delta$ construct, Greg Hura for help with SAXS data collection, and Mark Kelly for help with NMR. Funding for this project was provided by the Howard Hughes Medical Institute. T.O.S. was supported by a Damon Runyon Cancer Research Foundation fellowship. Many thanks to members of the Agard lab for helpful discussions.

Received: September 28, 2010

Revised: December 3, 2010

Accepted: January 7, 2011

Published: April 7, 2011

REFERENCES

- Alexandrescu, A.T., and Shortle, D. (1994). Backbone dynamics of a highly disordered 131 residue fragment of staphylococcal nuclease. *J. Mol. Biol.* 242, 527–546.
- Alexandrescu, A.T., Abeygunawardana, C., and Shortle, D. (1994). Structure and dynamics of a denatured 131-residue fragment of staphylococcal nuclease: a heteronuclear NMR study. *Biochemistry* 33, 1063–1072.
- Ali, M.M., Roe, S.M., Vaughan, C.K., Meyer, P., Panaretou, B., Piper, P.W., Prodromou, C., and Pearl, L.H. (2006). Crystal structure of an Hsp90-nucleotide-p23/Sba1 closed chaperone complex. *Nature* 440, 1013–1017.
- Baskakov, I., and Bolen, D.W. (1998). Forcing thermodynamically unfolded proteins to fold. *J. Biol. Chem.* 273, 4831–4834.
- Bron, P., Giudice, E., Rolland, J.P., Buey, R.M., Barbier, P., Diaz, J.F., Peyrot, V., Thomas, D., and Garnier, C. (2008). Apo-Hsp90 coexists in two open conformational states in solution. *Biol. Cell* 100, 413–425.
- Cunningham, C.N., Krukenberg, K.A., and Agard, D.A. (2008). Intra- and inter-monomer interactions are required to synergistically facilitate ATP hydrolysis in Hsp90. *J. Biol. Chem.* 283, 21170–21178.
- Delaglio, F., Grzesiek, S., Vuister, G.W., Zhu, G., Pfeifer, J., and Bax, A. (1995). NMRPipe: a multidimensional spectral processing system based on UNIX pipes. *J. Biomol. NMR* 6, 277–293.
- Dollins, D.E., Warren, J.J., Immormino, R.M., and Gewirth, D.T. (2007). Structures of GRP94-nucleotide complexes reveal mechanistic differences between the hsp90 chaperones. *Mol. Cell* 28, 41–56.
- Falsone, S.F., Kungl, A.J., Rek, A., Cappai, R., and Zangger, K. (2009). The molecular chaperone Hsp90 modulates intermediate steps of amyloid assembly of the Parkinson-related protein alpha-synuclein. *J. Biol. Chem.* 284, 31190–31199.
- Forsythe, H.L., Jarvis, J.L., Turner, J.W., Elmore, L.W., and Holt, S.E. (2001). Stable association of hsp90 and p23, but not hsp70, with active human telomerase. *J. Biol. Chem.* 276, 15571–15574.
- Hessling, M., Richter, K., and Buchner, J. (2009). Dissection of the ATP-induced conformational cycle of the molecular chaperone Hsp90. *Nat. Struct. Mol. Biol.* 16, 287–293.
- Jakob, U., Lilie, H., Meyer, I., and Buchner, J. (1995). Transient interaction of Hsp90 with early unfolding intermediates of citrate synthase. Implications for heat shock in vivo. *J. Biol. Chem.* 270, 7288–7294.
- Krukenberg, K.A., Förster, F., Rice, L.M., Sali, A., and Agard, D.A. (2008). Multiple conformations of E. coli Hsp90 in solution: insights into the conformational dynamics of Hsp90. *Structure* 16, 755–765.
- Krukenberg, K.A., Böttcher, U.M., Southworth, D.R., and Agard, D.A. (2009a). Grp94, the endoplasmic reticulum Hsp90, has a similar solution conformation to cytosolic Hsp90 in the absence of nucleotide. *Protein Sci.* 18, 1815–1827.
- Krukenberg, K.A., Southworth, D.R., Street, T.O., and Agard, D.A. (2009b). pH-dependent conformational changes in bacterial Hsp90 reveal a Grp94-like conformation at pH 6 that is highly active in suppression of citrate synthase aggregation. *J. Mol. Biol.* 390, 278–291.
- McLaughlin, S.H., Smith, H.W., and Jackson, S.E. (2002). Stimulation of the weak ATPase activity of human hsp90 by a client protein. *J. Mol. Biol.* 315, 787–798.
- Mickler, M., Hessling, M., Ratzke, C., Buchner, J., and Hugel, T. (2009). The large conformational changes of Hsp90 are only weakly coupled to ATP hydrolysis. *Nat. Struct. Mol. Biol.* 16, 281–286.
- Motojima-Miyazaki, Y., Yoshida, M., and Motojima, F. (2010). Ribosomal protein L2 associates with E. coli HtpG and activates its ATPase activity. *Biochem. Biophys. Res. Commun.* 400, 241–245.

- Ohnishi, S., and Shortle, D. (2003). Effects of denaturants and substitutions of hydrophobic residues on backbone dynamics of denatured staphylococcal nuclease. *Protein Sci.* *12*, 1530–1537.
- Onuoha, S.C., Coulstock, E.T., Grossmann, J.G., and Jackson, S.E. (2008). Structural studies on the co-chaperone Hop and its complexes with Hsp90. *J. Mol. Biol.* *379*, 732–744.
- Rudiger, S., Freund, S.M., Veprintsev, D.B., and Fersht, A.R. (2002). CRINEPT-TROSY NMR reveals p53 core domain bound in an unfolded form to the chaperone Hsp90. *Proc. Natl. Acad. Sci. USA* *99*, 11085–11090.
- Schneider, C., Sepp-Lorenzino, L., Nimmesgern, E., Ouerfelli, O., Danishefsky, S., Rosen, N., and Hartl, F.U. (1996). Pharmacologic shifting of a balance between protein refolding and degradation mediated by Hsp90. *Proc. Natl. Acad. Sci. USA* *93*, 14536–14541.
- Shiau, A.K., Harris, S.F., Southworth, D.R., and Agard, D.A. (2006). Structural Analysis of *E. coli* hsp90 reveals dramatic nucleotide-dependent conformational rearrangements. *Cell* *127*, 329–340.
- Shortle, D. (2002). The expanded denatured state: an ensemble of conformations trapped in a locally encoded topological space. *Adv. Protein Chem.* *62*, 1–23.
- Shortle, D., and Meeker, A.K. (1989). Residual structure in large fragments of staphylococcal nuclease: effects of amino acid substitutions. *Biochemistry* *28*, 936–944.
- Southworth, D.R., and Agard, D.A. (2008). Species-dependent ensembles of conserved conformational states define the Hsp90 chaperone ATPase cycle. *Mol. Cell* *32*, 631–640.
- Street, T.O., Krukenberg, K.A., Rosgen, J., Bolen, D.W., and Agard, D.A. (2010). Osmolyte-induced conformational changes in the Hsp90 molecular chaperone. *Protein Sci.* *19*, 57–65.
- Svergun, D. (1991). Mathematical models in small-angle scattering data analysis. *J. Appl. Cryst.* *24*, 485–492.
- Svergun, D.I. (1999). Restoring low resolution structure of biological macromolecules from solution scattering using simulated annealing. *Biophys. J.* *76*, 2879–2886.
- Taipale, M., Jarosz, D.F., and Lindquist, S. (2010). HSP90 at the hub of protein homeostasis: emerging mechanistic insights. *Nat. Rev. Mol. Cell Biol.* *11*, 515–528.
- Vaughan, C.K., Gohlke, U., Sobott, F., Good, V.M., Ali, M.M., Prodromou, C., Robinson, C.V., Saibil, H.R., and Pearl, L.H. (2006). Structure of an Hsp90-Cdc37-Cdk4 complex. *Mol. Cell* *23*, 697–707.
- Wang, Y., and Shortle, D. (1995). The equilibrium folding pathway of staphylococcal nuclease: identification of the most stable chain-chain interactions by NMR and CD spectroscopy. *Biochemistry* *34*, 15895–15905.
- Wang, Y., Alexandrescu, A.T., and Shortle, D. (1995). Initial studies of the equilibrium folding pathway of staphylococcal nuclease. *Philos. Trans. R. Soc. Lond. B Biol. Sci.* *348*, 27–34.
- Wiech, H., Buchner, J., Zimmermann, R., and Jakob, U. (1992). Hsp90 chaperones protein folding in vitro. *Nature* *358*, 169–170.
- Young, J.C., Moarefi, I., and Hartl, F.U. (2001). Hsp90: a specialized but essential protein-folding tool. *J. Cell Biol.* *154*, 267–273.
- Zhang, W., Hirshberg, M., McLaughlin, S.H., Lazar, G.A., Grossmann, J.G., Nielsen, P.R., Sobott, F., Robinson, C.V., Jackson, S.E., and Laue, E.D. (2004). Biochemical and structural studies of the interaction of Cdc37 with Hsp90. *J. Mol. Biol.* *340*, 891–907.